SCIENCE CHINA
Information Sciences

• RESEARCH PAPER •

July 2024, Vol. 67, Iss. 7, 172401:1–172401:10
https://doi.org/10.1007/s11432-023-3938-y

Highly sensitive flexible strain sensor based on the two-dimensional semiconductor tellurium with a negative gauge factor

Jiarui HE[1,2†], Yusong QU[3†], Shengyao CHEN[3], Cong WANG[1*], Lena DU[4*], Xiaoshan DU[3], Yuanyuan ZHENG[1], Guozhong ZHAO[4] & He TIAN[2*]

[1]*College of Mathematics and Physics, Beijing University of Chemical Technology, Beijing* 100029, *China;*
[2]*School of Integrated Circuits, Tsinghua University, Beijing, China & The Beijing National Research Center for Information Science and Technology (BNRist), Tsinghua University, Beijing* 100084, *China;*
[3]*CAS Center for Excellence in Nanoscience, National Center for Nanoscience and Technology & University of Chinese Academy of Sciences, Beijing* 100190, *China;*
[4]*Beijing Key Lab of Terahertz Spectroscopy and Imaging, Key Lab of Terahertz Optoelectronics, Ministry of Education, Department of Physics, Capital Normal University, Beijing* 100048, *China*

Received 6 September 2023/Revised 17 October 2023/Accepted 13 December 2023/Published online 13 June 2024

Abstract Research on flexible strain sensors has advanced rapidly in recent years, with particular attention being devoted to two-dimensional (2D) semiconductor materials owing to their exceptional mechanical and electrical properties that are conducive to sophisticated sensing performance. However, resistive strain sensors based on 2D semiconductor materials typically exhibit positive gauge factors (GF), while materials for strain sensors with a negative GF remain elusive. We have identified a trend of reduction in the band gap of the emerging 2D semiconductor material tellurium (Te) under strain in simulations reported in past research, and have observed a negative GF in the Te-based strain sensor. In this study, we combined Te with a flexible polyethylene terephthalate (PET) substrate to manufacture a flexible strain sensor with a significantly negative GF. The results of tests revealed that the Te-based strain sensor achieved an impressive maximum sensitivity of −139.7 within a small range of bending-induced strain (< 1%). Furthermore, it exhibited excellent linearity and good cyclic stability, and was successfully applied to monitor limb movements. The work here verifies the significant potential for the use of Te-based strain sensors in next-generation flexible electronics.

Keywords 2D semiconductor materials, 2D tellurium, flexible electronics, strain sensors, negative gauge factor, high sensitivity

1 Introduction

Flexible strain sensors are functional devices that measure strain-related stimuli by detecting changes in electrical signals caused by stress. Commonly used strain sensors can be broadly categorized based on their mechanisms of sensing, and include resistive, piezoelectric, capacitive, and frictional strain sensors [1]. Resistive strain sensors, which operate on the basic principle of detecting strain-related stimuli through changes in the resistance of the device, are among the most widely used sensors due to their advantages of a simple structure, low energy consumption, easy readout, and wide range of detection [2,3]. Currently used commercial resistive strain sensors primarily use metal materials, but the lack of a band gap in such materials typically limits their gauge factor (GF) to a relatively narrow range to significantly restrict their applications in the field of strain sensing. By contrast, semiconductor materials exhibit significant changes in their resistivity when subjected to pressure owing to their larger band gap, because of which

* Corresponding author (email: wangcongphysics@mail.buct.edu.cn, duln@cnu.edu.cn, tianhe88@tsinghua.edu.cn)
† He J R and Qu Y S have the same contribution to this work.

strain sensors based on semiconductor materials have a higher sensitivity than metal-based strain sensors. Nevertheless, traditional three-dimensional (3D) semiconductor materials (such as Si, Ge, and GaAs) often cannot withstand large strains without incurring damage, where this significantly limits their range of strain detection in wearable devices and poses a major obstacle to the application of semiconductors to strain sensors.

Two-dimensional (2D) semiconductor materials, with graphene as a representative, have attracted unprecedented research interest in recent years owing to their atomic-level thickness and excellent optoelectronic properties [4–6]. Moreover, 2D semiconductors often exhibit excellent mechanical properties that enable them to withstand a significant magnitude of strain without damage [7]. Their excellent characteristics of piezoelectric coupling have lately led to a flurry of research on flexible strain sensors based on 2D semiconductor materials [8]. Resistive strain sensors based on 2D semiconductor materials typically tend to have a positive GF, and numerous studies have been conducted on positive strain sensors based on low-dimensional carbon materials such as graphene [9, 10]. However, the application of strain sensors based on 2D semiconductors with a positive GF encounters some limitations. Strain sensors with a negative GF can be used to measure both positive and negative strains in certain applications. For instance, when an object is subjected to compression, strain sensors with a negative GF are more suitable for conducting measurements because they exhibit a more pronounced increase in resistance and a wider range of detection of strain induced by a negative response. Sensors with a negative GF can be applied in conjunction with those with a positive GF in some scenarios to conduct relative measurements of strain. However, few studies have examined strain sensors based on 2D semiconductors that use a negative GF. Moreover, the relevant values are generally small even if a negative GF is obtained. Therefore, the exploration of strain sensors based on 2D semiconductors with a significantly negative GF has emerged as an important scientific problem in the field of 2D semiconductor-based strain sensors in recent years.

Of the various 2D semiconductor materials, Te has been recently identified as a promising p-type 2D semiconductor material [11]. It is characterized by its anisotropic atomic structure [12, 13], excellent transport-related properties (demonstrating ultra-high hole mobility of up to $\sim$1000 $\mathrm{cm^2{\cdot}V^{-1}{\cdot}s^{-1}}$ at room temperature) [14–17], and good optoelectronic characteristics and stability, where this makes it a promising candidate material for use in next-generation electronic and photonic devices [18–22]. More importantly, the unique helical chain and symmetry-breaking structure of the Te semiconductor confer advantages in terms of its piezoresistive and piezoelectric effects. Wang et al. [23] studied the introduction of pre-strain to induce corrugated structures in 2D Te, and explored its feasibility as a high gain factor for ultra-stretchable sensors. Li et al. [15] used Te nanowires (NWs) to modulate the electronic structure and piezoelectric polarization, and developed a dual-sensing method of signal decoupling for indications of the temperature and pressure. These factors attest to the promise of investigating strain sensors based on 2D Te semiconductors.

We chose a 2D semiconductor material, Te nanomaterial, as the object of this study because it exhibits a distinctive trend in simulations such that its band gap energy gradually decreases with a small increase in the stretching-induced strain (decreasing compressive strain). This behavior leads to an increase in its conductivity and a decrease in its resistance, thus aligning with the characteristics of a sensor with a negative GF. To validate our hypothesis, we applied a flexible substrate (polyethylene terephthalate, PET) and used a simple process of fabrication to create flexible strain sensors by using 2D Te samples. We applied a different method of substrate bending than those used in previously reported approaches to apply the strain. The resulting sensors demonstrated excellent performance in terms of bending-induced strain. Their resistance exhibited a gradual decrease with increasing bending strain under various values of the latter while also generating a high negative GF. This is different from the procedure used in a previous study, in which another method for the application of strain (substrate pre-stretching) was used, and resulted in a positive GF yielded by the Te-based sensor [23]. This alignment between the experimental results and the simulated trends confirmed our hypothesis. Furthermore, the proposed strain sensor exhibited high sensitivity within a small range of bending strain, thus displaying an excellent linear relationship with the bending strain and showcasing sound cyclic stability under multiple strain cycles. Finally, the application of this device to monitor limb movement validated its potential for health monitoring, gesture recognition, motion tracking, and related tasks. The work here demonstrates the promising role of the 2D semiconductor Te in strain sensors with a negative GF.

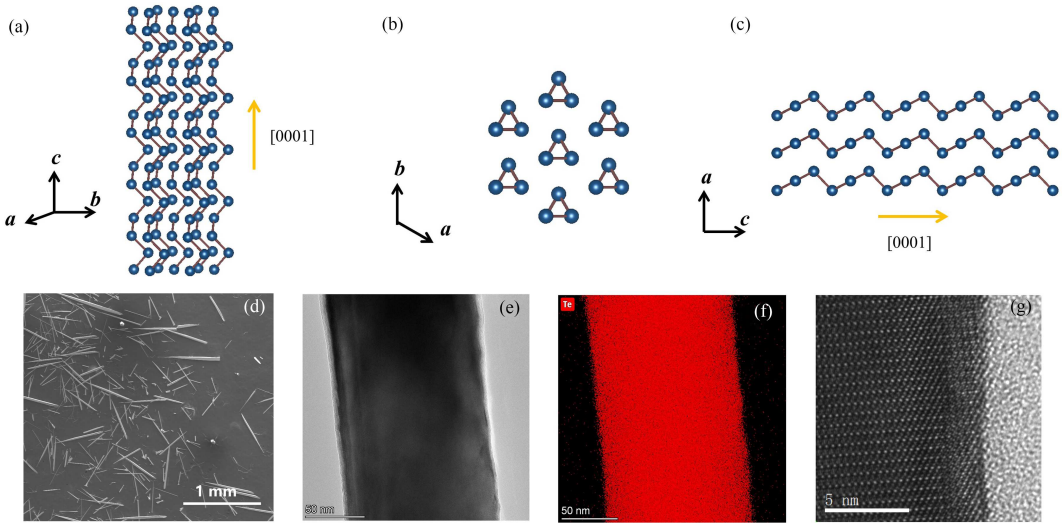

Figure 1 Atomic structure of (a) Te, (b) Te viewed from the *c*-axis, and (c) Te viewed from the *b*-axis; (d) SEM image of 2D Te synthesized via the PVD method; (e) TEM image of the localized 2D Te nanomaterial; (f) image of the TEM-based EDS mapping of the localized 2D Te nanomaterial; (g) HR-TEM image of the 2D Te nanomaterial.

2 Materials and methods

2.1 Characteristics of tellurium

2D Te is an emerging narrow-band gap semiconductor material, as shown in Figures 1 (a)–(c). It consists of triangular helical atomic chains that are stacked together through van der Waals forces to form a hexagonal lattice structure, and exhibits triple helical symmetry along the [0001] direction. Furthermore, Te atoms form only covalent bonds with two adjacent atoms in the helical chain, where this contrasts sharply with traditional 2D semiconductor materials such as graphene and black phosphorus (BP), which have strong chemical bonds in their layered structures. A sawtooth-like layering can be observed along the *b*-axis [23,24]. The structure of 2D Te exhibits significant anisotropy that lends uncommon anisotropic optical and electrical properties to the material. We applied the physical vapor deposition (PVD) technique to cause Te to evaporate and deposit it onto the surfaces of silicon wafers or silicon dioxide. This allowed us to ultimately obtain 2D Te nanomaterials within a horizontal vacuum tube furnace. Figures 1(d) and (e) show the scanning electron microscope (SEM) and localized transmission electron microscope (TEM) images of the synthesized material, respectively. It is evident from them that the synthesized 2D Te materials had a ribbon-like structure, with lengths ranging from tens to hundreds of micrometers and widths in the tens of nanometers. The long, straight edges of the Te material are always aligned parallel to the [0001] direction of the crystal. This geometric anisotropy enables the quick determination of its crystallographic orientation without requiring other, more complex, methods. The energy-dispersive spectrometer (EDS) mapping shown in Figure 1(f) confirmed that the synthesized nanomaterial consisted solely of Te, and the 2D Te exhibited a uniform quality. Moreover, Figure 1(g) shows a high-resolution transmission electron microscope (HR-TEM) image that clearly shows the defect-free hexagonal lattice structure of Te, reflecting the high quality of the synthesized material.

2.2 Working mechanism

In order to gain a comprehensive understanding of the working mechanisms of 2D Te materials under strain, we investigated their structural properties when subjected to strain. We initially performed Raman spectroscopy tests on 2D Te when subjected to various small strains. The results revealed two characteristic vibrational modes, as shown in Figure 2(a), known as A^1 and E^2. The most prominent Raman peak associated with the A^1 mode was observed at approximately 120 cm^{-1}, corresponding to the chain-extension mode in which each atom moved within the basal plane. The E^2 mode, located around 140 cm^{-1}, primarily resulted from the asymmetric stretching of atoms along the *c*-axis [25]. Under strains of 0%, 0.5%, and 0.7%, the Raman peaks of the A^1 mode were observed at 118.2, 117.3, and 116.3 cm^{-1}, respectively, while the Raman peaks of the E^2 mode were located at 138.3, 137.8, and

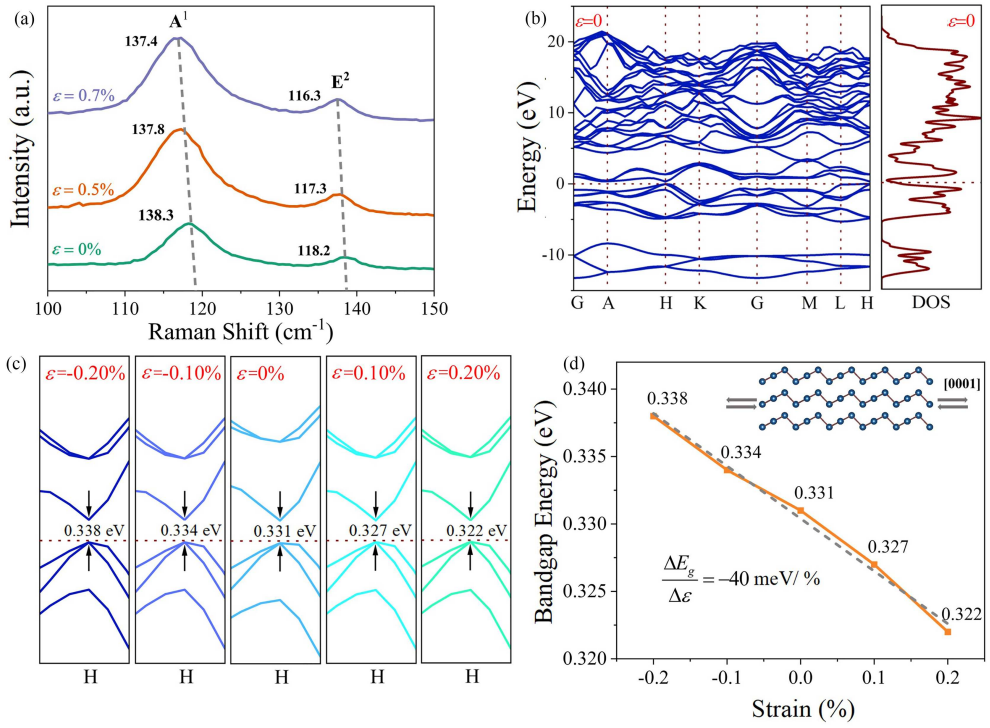

Figure 2 (a) Raman spectra of the Te sensor under no strain, 0.5% strain, and 0.7% strain; (b) diagrams of the band structure and density of states (DOS) of Te with a biaxial strain of zero, obtained through DFT; (c) diagrams of the band structure of Te under uniaxial compressive or stretching-induced strains of −0.20%, −0.10%, 0%, 0.10%, and 0.20%; (d) variations in the band gap of the Te nanomaterials when a small strain was applied.

137.4 cm^{-1}, respectively. Both the A^1 and the E^2 modes exhibited a slight downshift in frequency under the influence of strain compared with the unstrained sample. These changes in the vibrational frequencies of the lattice indicated that the strain had modulated the lattice structure of the Te nanomaterial, potentially resulting in alterations in the resistance of Te-based strain sensors.

The band gap varied linearly with the strain under small magnitudes of the latter. The change in the conductivity of the semiconductor material with strain can be expressed as [26]

$$G(\varepsilon) = G(0)\exp\left[-\frac{\varepsilon}{2k_BT}\frac{\partial E_g}{\partial \varepsilon}\right], \tag{1}$$

where $G(\varepsilon)$ and $G(0)$ represent the conductivities under strain and in the initial state, respectively, k_B denotes the Boltzmann constant, T represents the temperature, and E_g represents the band gap energy of the material.

We also used density functional theory (DFT) to calculate the band structure of Te under both the absence of strain (Figure 2(b)) and a small uniaxial compressive or stretching-induced strain (−0.2%–0.2%). The results showed that the band gap gradually narrowed with increasing uniaxial strains of −0.20%, −0.10%, 0%, 0.1%, and 0.2% (Figure 2(c)). We further analyzed the relationship between the band gap energy and the strain, and it is evident from Figure 2(d) that the reduction in the former followed an almost linear trend with increasing values of the latter. Moreover, $\frac{\partial E_g}{\partial \varepsilon} = -40$ meV/%. By substituting this into (1), it becomes evident that the conductivity of 2D Te increased with the small uniaxial compressive or stretching-induced strain, resulting in a reduction in its resistance. These outcomes indicated that the electronic band structure of 2D Te underwent certain changes under the influence of uniaxial strain. The band gap gradually decreased as the uniaxial strain increased, and this continually enhanced the likelihood of electron transitions near the Fermi energy level. This leads in turn to an increase in the conductivity of the corresponding strain-sensitive devices and a reduction in resistance, and shows the potential for the use of the 2D semiconductor Te to monitor positive and negative stresses. Consequently, we think that strain sensors based on the 2D semiconductor Te possess a negative GF.

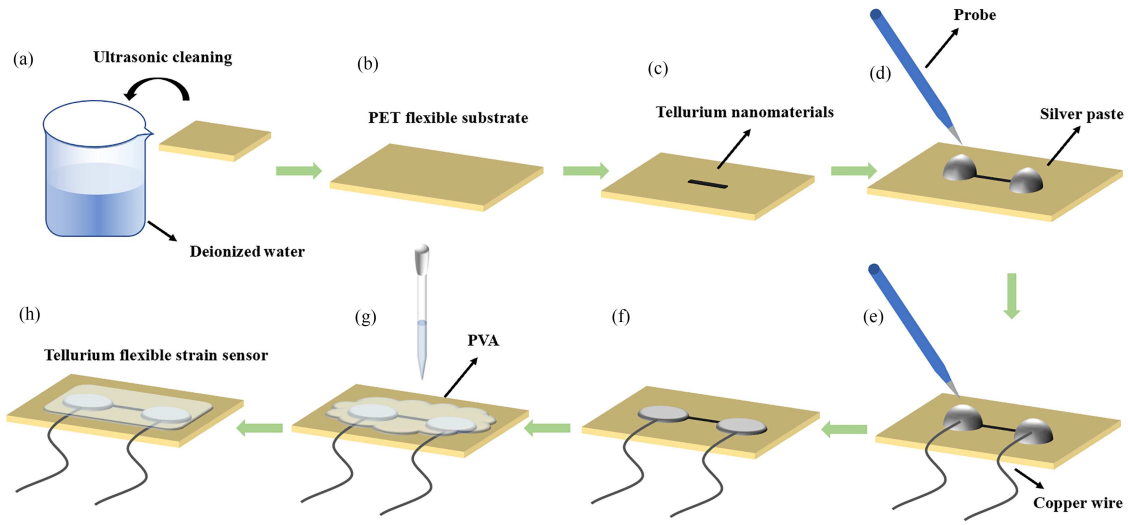

Figure 3 (a) The pre-cut PET was subjected to ultrasonic cleaning; (b) the PET substrate was placed in the environment of an inert gas; (c) Te nanomaterials were transferred to the center of the PET substrate; (d) silver paste was picked up and connected to both ends of the 2D Te to act as electrodes; (e) copper wires were fixed on the ends of the electrodes; (f) the PET substrate was placed in an oven and dried; (g) PVA solution was dripped onto the substrate; (h) PVA was dried at room temperature.

2.3 Device fabrication

The process of preparing a strain sensor based on Te consists of several steps, the important ones of which are shown in Figure 3. The pre-cut PET substrate was placed in a beaker containing deionized water, and was subjected to ultrasonic cleaning to remove impurities and dirt from the surface. The PET substrate was then placed in the environment of an inert gas, such as nitrogen (N_2), and dried to ensure that its surface was completely dry. High-quality Te nanomaterials were then selected and transferred to the center of the PET substrate under a microscope, with the long edges of Te parallel to those of the PET. Subsequently, a small amount of silver paste was picked up with a probe and connected to both ends of the 2D Te to act as electrodes. Similarly, copper wires were fixed on the ends of the electrodes by using this silver paste. Both these steps were performed under a microscope. The PET substrate, with the connected electrodes and silver wires, was placed in an oven and dried at 90°C for 1 h to cure the silver paste and improve its conductivity. Following this, a prepared polyvinyl alcohol (PVA) solution was dripped onto the substrate to cover the electrodes and the sensing material (2D Te). The purpose was to enhance adhesion among the Te material, electrodes, and the substrate under strain to prevent slipping [27]. Finally, the PVA was allowed to dry at room temperature. With this step, the fabrication of the strain sensor based on the 2D semiconductor Te was complete.

2.4 Measurement

We used a programmable RIGOL DM3068 digital multimeter, a high-precision electronic universal material testing machine from Shimadzu, and a vernier caliper to test the performance of the proposed sensor. The multimeter sampled the resistance of the device at a frequency of 50 Hz. To apply strain to the sensors, we combined the device with the stretching apparatus of the material testing machine. The two ends of the strain sensor were fixed to the two ends of the stretching apparatus in an initial horizontal position during testing. One end of the stretching platform remained fixed while the other end could be moved to different distances through a control panel, as shown in Figures 4(a) and (b). The distance between the ends of the stretching platform was L_0 in the initial state. After moving one end of the stretching platform at a certain distance, the distance between the ends became L, and the height of the raised PET flexible substrate was h. We conducted a mechanical simulation to visually understand the stress distribution in the PET substrate under bending strain. We constructed a model that combined a PET substrate and a tensile testing apparatus (the size of the substrate was 3 cm × 2 cm × 0.1 cm), with one end of the apparatus fixed, and a small, inward displacement (0.5 cm) applied at the other end. The stress distribution of the substrate under the static condition as well as that of linear buckling is shown in Figure 4(c). The middle region of the PET plate underwent significant tensile strain under the

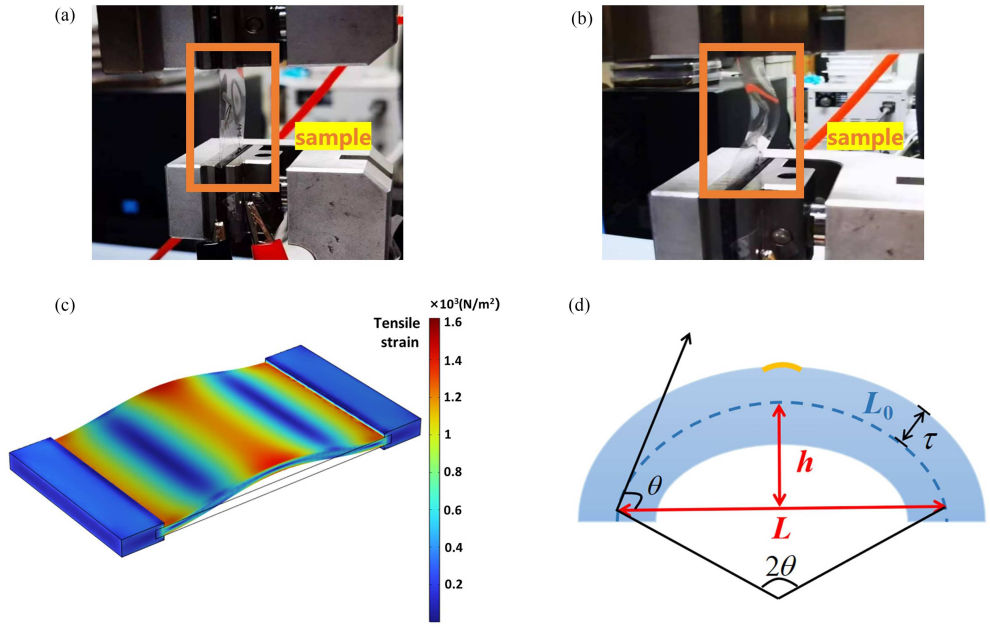

Figure 4 (a) Device combined with the stretching stage before applying strain; (b) bending strain of the device as the stretching stage moved; (c) mechanical simulation of the PET substrate under bending strain; (d) physical illustration of the calculation of the bending strain on the PET substrate.

bending condition. Therefore, when transferring the sample to the PET substrate, the material should be placed parallel to the central area to withstand noticeable strain-induced stimulation.

The physical computational model is illustrated in Figure 4(d). The strain on the upper surface of the PET can be calculated using [28]:

$$\varepsilon = \frac{\tau}{R} = \frac{2\tau \sin\theta}{L}, \tag{2}$$

where ε represents the strain on the upper surface of the PET, L denotes the distance between the ends after applying strain to the flexible substrate, L is the initial distance between the ends, R is the radius of curvature, τ is half of the thickness of the PET substrate, and θ is the tangent to the bending strain, and could be determined by measuring the angular relationship between L and h by using the vernier caliper.

3 Discussion

3.1 Performance of the sensor

The experimental current-voltage curve obtained within a range of bending strains of 0%–0.5% is presented in Figure 5(a), while Figure 5(b) shows changes in the resistance of the sensor upon the application of each magnitude of the strain within a range not exceeding 1%. Based on these data, we can deduce that the resistance of the device consistently decreased with an increase in the bending strain, reflecting the effectiveness of the sensor in detecting various degrees of bending strain. Sensitivity, which is a crucial performance-related parameter of a strain sensor, can be calculated as follows:

$$\mathrm{GF} = [(R - R_0)/R_0]/\varepsilon. \tag{3}$$

As previously mentioned, we observed that the device exhibited a monotonically decreasing relative resistance within the range of bending strain of 0%–0.91%, as shown in Figure 5(c). Specifically, GF_1 was as high as -139.7 within the range of bending strain of 0%–0.40%, while GF_2 was approximately -45.4 with the range of bending strain of 0.4%–0.91%. In both cases, we observed excellent linearity ($R^2 = 0.99$) with outstanding linear fitting, indicating the reliable and predictable performance of the strain sensor across this range of strain. It is thus evident that the sensor exhibited a relatively rare negative GF. We can surmise that this sensor exhibits a better zero-point calibration and stability than

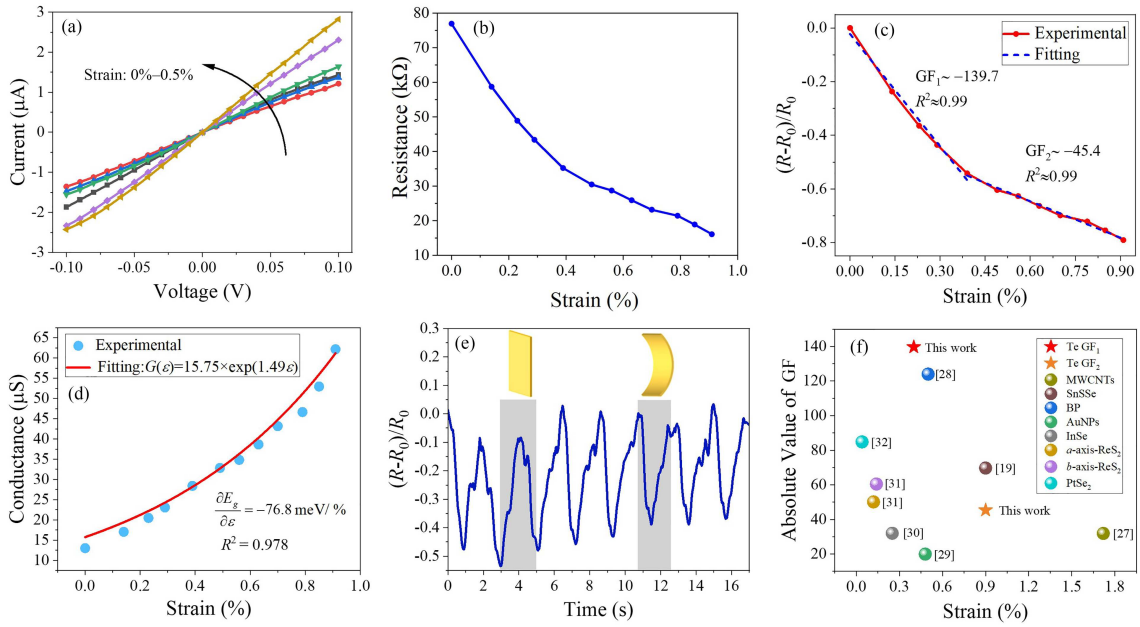

Figure 5 (a) *I-V* curves of the sensor under different bending strains, with electrical measurements conducted at voltages ranging from −0.1 to 0.1 V; (b) values of resistance of the sensor under different bending strains; (c) the trend of the relative changes in the resistance of the strain sensor with respect to the applied strain, with a value of $GF_1 \sim -139.7$ for strains ranging from 0% to 0.40%, and that of $GF_2 \sim -45.4$ for strains from 0.4% to 0.91% through linear fitting; (d) fitting of the changes in the conductivity of the device under different bending strains based on the theoretical model; (e) relative resistance-related response of the sensor under a bending strain of approximately 0.5%, applied in eight consecutive cycles; (f) comparison of the performance of sensors formed by using a single material under slight bending strains.

sensors with a positive GF because a change in the absolute value of the relative resistance of a sensor with a negative GF is always limited to within the range of zero to one. We used experimental data to verify the results of simulations of the DFT mentioned above. We performed a fitting analysis on changes in the conductivity of the 2D semiconductor material Te under a range of strain of 0% to 0.91%, as shown in Figure 5(d), and obtained the fitted function $G(\varepsilon) = 15.75 \times \exp(1.49\varepsilon)$ according to (1). The degree of fitting, R^2, was approximately 0.978, indicating a highly favorable fit that aligned with the proposed theoretical model. Moreover, the band gap energy of the semiconductor Te contracted under tensile strain at the rate of −76.8 meV/%. This shows that the observed experimental phenomenon was consistent with the trend of simulations of the reduced band gap under uniaxial strain, as shown in Figure 2(c). This provides an explanation for the negative GF observed in strain sensors based on the 2D semiconductor Te.

We also conducted multiple cycles of tests of bending strains of the same magnitude on the flexible sensor to evaluate its stability and the repeatability of its results. Figure 5(e) shows that its resistance-related response followed similar trends in each cycle, indicating its outstanding consistency. This suggests that it is suitable for use in dynamic strain monitoring.

To comprehensively evaluate the performance of our sensor, we analyzed it in comparison with strain sensors developed in recent years that are based on a variety of single materials, including carbon, metallic materials, and other common 2D materials as illustrated in Table 1 [24, 29–40]. The findings suggest that the proposed strain sensor, which uses the 2D semiconductor Te, yielded a relatively rare trend of a negative GF as the band gap energy decreased with increasing strain, especially at low values of strain. Its absolute value of the GF was as high as 139.7. It significantly outperformed strain sensors based on carbon materials like graphene as well as those based on metal nanoparticles (NPs) and NWs. Furthermore, it delivered a superior absolute value of the GF compared with sensors composed of other 2D materials, including BP, InSe, ReS_2, and MXene, where this highlights its excellent performance in terms of detection. We also conducted a lateral comparison of its performance under a small bending strain on the substrate (no more than 2%, and mostly within 1%), and the results are depicted in Figure 5(f). The proposed sensor achieved a higher absolute value of the GF compared with strain sensors made of other single materials within a narrow range of detection (0%–0.40%). Moreover, it maintained a substantially high sensitivity of detection within the range of strain of 0.4%–0.91%. These results further

Table 1 Comparison of the performance of strain sensors based on different materials

Materials	Strain-inducing methods	Sensing scale (%)	Maximum GF value	Ref.
SWCNT	Substrate stretching	100	72	[29]
AgNWs	Substrate stretching	70	14	[30]
AuNWs	Substrate stretching	25	7.34	[31]
MXene	Substrate stretching	20	24.35	[32]
GaSe	Substrate pre-stretching	20	−4.3	[33]
Graphene	Indentation	3	1.9	[34]
MWCNTs	Substrate bending	1.72	31.9	[35]
Te	Substrate bending	0.9	−139.7	This work
SnSSe	Substrate bending	0.9	69.7	[24]
BP	Substrate bending	0.5	124	[36]
AuNPs	Substrate bending	0.48	19.94	[37]
InSe	Substrate bending	0.25	32	[38]
b-axis-ReS_2	Substrate bending	0.14	−60.49	[39]
a-axis-ReS_2	Substrate bending	0.12	50.14	[35]
$PtSe_2$	Substrate bending	0.04	−84.8	[40]

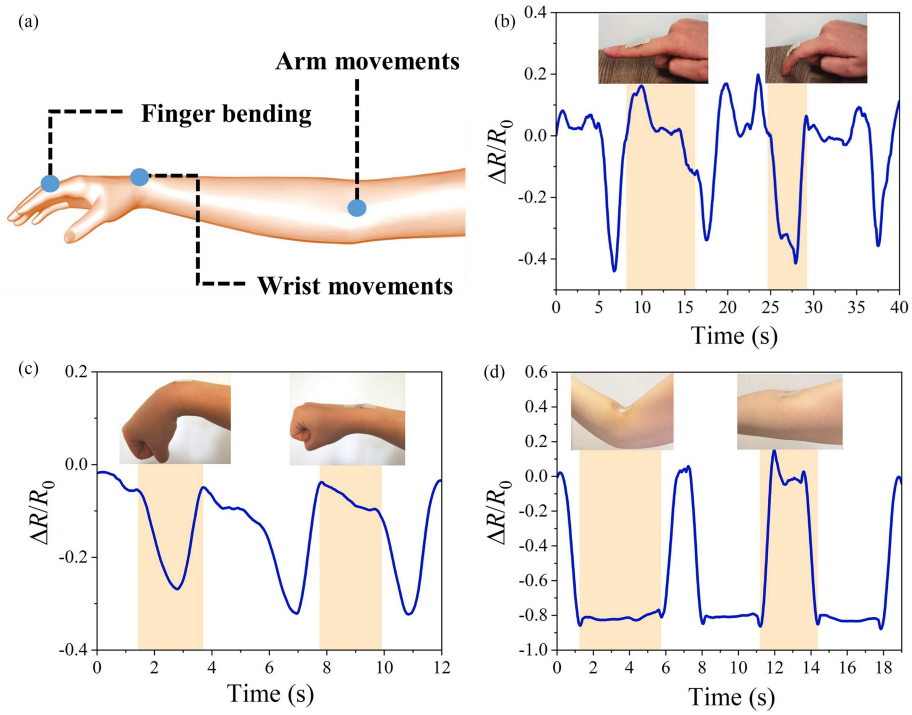

Figure 6 (a) Use of the proposed sensor to monitor the motion of the upper limb. Changes in the relative resistance detected by the sensor during different states of motion of (b) the finger, (c) wrist, and (d) forearm, respectively.

demonstrate the outstanding performance of our sensor, and attest to its promise for use in applications that require sensitive and reliable detection of strain.

3.2 Detection of human motion

The application of flexible strain sensors has been demonstrated in a diversity of fields in recent years, including health monitoring, gesture recognition, and motion tracking. We accordingly examined the performance of our strain sensor based on the 2D semiconductor Te in such applications. By affixing it to various joints of the human upper limb, we monitored the resistance-related response of the device in realtime to reflect the movements of the limbs. The locations of measurement are illustrated in Figure 6(a), and the results of monitoring are shown in Figures 6 (b)–(d).

When we attached our sensor to the second joint of the right index finger and monitored its response while the finger was bent and tapped on a desktop, the results exhibited multiple prominent downward

peaks in its relative resistance-related response during the repetitive tapping actions. This confirmed the effectiveness of the sensor in providing real-time feedback on the bending motion of the finger. Subsequently, we placed the sensor on the wrist to monitor its downward bending motions. Throughout multiple cycles of wrist movement, the resistance of the sensor changed consistently, signifying a reliable response to the motion of the wrist. Similarly, when we attached the sensor to the forearm to monitor its flexion and extension, the results also reflected the accurate real-time monitoring capabilities of our strain sensor in response to forearm motion. These applications clearly showcase the capabilities of our strain sensor. It provided relatively stable detection for both the forward (motion) and the reverse process (recovery), making it a highly promising candidate for use in wearable devices and motion-related monitoring systems.

4 Conclusion

We considered the emerging 2D semiconductor Te as the object of research in this study. We discovered through theoretical formulae and first-principles calculations that the band gap and resistance of Te decreased under strain, reflecting the characteristics of a sensor with a negative GF. Following this, we applied a cost-effective and convenient technique of fabrication to create strain sensors based on Te with a negative sensitivity factor. Within the range of bending strain of 0%–0.9%, the maximum absolute value of its measured GF was as high as 139.7. The results of comparisons with other sensors showed that it has a higher sensitivity of detection under small bending strains. Moreover, the proposed sensor demonstrated excellent repeatability. We also applied it to monitor limb movement as well as for gesture recognition and motion tracking. The results of this study showed that the 2D semiconductor Te holds significant promise as a valuable material in the realm of strain sensors with a negative GF. Furthermore, it has the potential to surpass the limitations of sensors with a positive GF in terms of detecting negative strain, zero-point calibration, and stability. We expect future work in the area to focus on combining sensors with negative and positive GFs to provide an even more accurate detection of strain signals.

Acknowledgements This work was supported by National Natural Science Foundation of China (Grant Nos. 62205011, 52302189, 62374099), Tsinghua-Toyota Joint Research Fund, Beijing Natural Science Foundation-Xiaomi Innovation Joint Fund (Grant No. L233009), Fundamental Research Funds for the Central Universities (Grant No. buctrc202122), and R&D Program of Beijing Municipal Education Commission (Grant No. KM202310028013).

References

1 Pyo S, Lee J, Bae K, et al. Recent progress in flexible tactile sensors for human-interactive systems: from sensors to advanced applications. Adv Mater, 2021, 33: e2005902
2 Duan L, D'hooge D R, Cardon L. Recent progress on flexible and stretchable piezoresistive strain sensors: from design to application. Prog Mater Sci, 2020, 114: 100617
3 Wan Y, Wang Y, Guo C F. Recent progresses on flexible tactile sensors. Mater Today Phys, 2017, 1: 61–73
4 Wang F, Wang Z, Jiang C, et al. Progress on electronic and optoelectronic devices of 2D layered semiconducting materials. Small, 2017, 13: 1604298
5 Wang C, Xiao R C, Liu H, et al. Room-temperature third-order nonlinear Hall effect in Weyl semimetal $TaIrTe_4$. Natl Sci Rev, 2022, 9: nwac020
6 Zha J, Shi S, Chaturvedi A, et al. Electronic/optoelectronic memory device enabled by tellurium-based 2D van der Waals heterostructure for in-sensor reservoir computing at the optical communication band. Adv Mater, 2023, 35: 2211598
7 Cao G, Gao H. Mechanical properties characterization of two-dimensional materials via nanoindentation experiments. Prog Mater Sci, 2019, 103: 558–595
8 Sun W, Wu F. Two-dimensional materials for antimicrobial applications: graphene materials and beyond. Chem An Asian J, 2018, 13: 3378–3410
9 Fu X W, Liao Z M, Zhou J X, et al. Strain dependent resistance in chemical vapor deposition grown graphene. Appl Phys Lett, 2011, 99: 213107
10 Wang Y, Yang R, Shi Z, et al. Super-elastic graphene ripples for flexible strain sensors. ACS Nano, 2011, 5: 3645–3650
11 Wang Y, Qiu G, Wang R, et al. Field-effect transistors made from solution-grown two-dimensional tellurene. Nat Electron, 2018, 1: 228–236
12 Kramer A, van de Put M L, Hinkle C L, et al. Tellurium as a successor of silicon for extremely scaled nanowires: a first-principles study. npj 2D Mater Appl, 2020, 4: 10
13 Reed E J. Two-dimensional tellurium. Nature, 2017, 552: 40–41
14 Li L, Wang D, Zhang D, et al. Near-infrared light triggered self-powered mechano-optical communication system using wearable photodetector textile. Adv Funct Mater, 2021, 31: 2104782
15 Li L, Zhao S, Ran W, et al. Dual sensing signal decoupling based on tellurium anisotropy for VR interaction and neuro-reflex system application. Nat Commun, 2022, 13: 5975
16 Yang P, Zha J, Gao G, et al. Growth of tellurium nanobelts on h-BN for p-type transistors with ultrahigh hole mobility. Nano-Micro Lett, 2022, 14: 109
17 Amani M, Tan C, Zhang G, et al. Solution-synthesized high-mobility tellurium nanoflakes for short-wave infrared photodetectors. ACS Nano, 2018, 12: 7253–7263

18 Yang Y, Xu M, Jia S, et al. A new opportunity for the emerging tellurium semiconductor: making resistive switching devices. Nat Commun, 2021, 12: 6081
19 Yan Z, Yang H, Yang Z, et al. Emerging two-dimensional tellurene and tellurides for broadband photodetectors. Small, 2022, 18: e2200016
20 Sharma S, Singh N, Schwingenschlögl U. Two-dimensional tellurene as excellent thermoelectric material. ACS Appl Energy Mater, 2018, 1: 1950–1954
21 Qiu G, Charnas A, Niu C, et al. The resurrection of tellurium as an elemental two-dimensional semiconductor. npj 2D Mater Appl, 2022, 6: 17
22 Zhao C, Tan C, Lien D H, et al. Evaporated tellurium thin films for p-type field-effect transistors and circuits. Nat Nanotechnol, 2020, 15: 53–58
23 Wang Y, Yao S, Liao P, et al. Strain-engineered anisotropic optical and electrical properties in 2D chiral-chain tellurium. Adv Mater, 2020, 32: e2002342
24 Shi Z, Cao R, Khan K, et al. Two-dimensional tellurium: progress, challenges, and prospects. Nano-Micro Lett, 2020, 12: 99
25 Du Y, Qiu G, Wang Y, et al. One-dimensional van der Waals material tellurium: Raman spectroscopy under strain and magneto-transport. Nano Lett, 2017, 17: 3965–3973
26 Neri I, López-Suárez M. Electronic transport modulation on suspended few-layer MoS_2 under strain. Phys Rev B, 2018, 97: 241408
27 Li Z, Lv Y, Ren L, et al. Efficient strain modulation of 2D materials via polymer encapsulation. Nat Commun, 2020, 11: 1151
28 Du L, Wang C, Xiong W, et al. Strain-induced band-gap tuning of 2D-SnSSe flakes for application in flexible sensors. Adv Mater Technol, 2020, 5: 1900853
29 Lee Y, Kim J, Hwang H, et al. Highly stretchable and sensitive strain sensors based on single-walled carbon nanotube-coated nylon textile. Korean J Chem Eng, 2019, 36: 800–806
30 Amjadi M, Pichitpajongkit A, Lee S, et al. Highly stretchable and sensitive strain sensor based on silver nanowire-elastomer nanocomposite. ACS Nano, 2014, 8: 5154–5163
31 Gong S, Schwalb W, Wang Y, et al. A wearable and highly sensitive pressure sensor with ultrathin gold nanowires. Nat Commun, 2014, 5: 3132
32 Yuan L, Zhang M, Zhao T, et al. Flexible and breathable strain sensor with high performance based on MXene/nylon fabric network. Sens Actuat A-Phys, 2020, 315: 112192
33 Wang C, Yang S X, Zhang H R, et al. Synthesis of atomically thin GaSe wrinkles for strain sensors. Front Phys, 2016, 11: 116802
34 Huang M, Pascal T A, Kim H, et al. Electronic-mechanical coupling in graphene from in situ nanoindentation experiments and multiscale atomistic simulations. Nano Lett, 2011, 11: 1241–1246
35 K T, Rajini G K, Maji D. Fully printed MWCNT strain sensor over paper substrate for human motion monitoring. Flex Print Electron, 2022, 7: 045003
36 Zhang Z, Li L, Horng J, et al. Strain-modulated bandgap and piezo-resistive effect in black phosphorus field-effect transistors. Nano Lett, 2017, 17: 6097–6103
37 Xu X L, Li S X, Yang Y, et al. High-performance strain sensor for detection of human motion and subtle strain by facile fabrication. Measurement, 2022, 189: 110658
38 Chen L, Yu Z G, Liang D, et al. Ultrasensitive and robust two-dimensional indium selenide flexible electronics and sensors for human motion detection. Nano Energy, 2020, 76: 105020
39 An C, Xu Z, Shen W, et al. The opposite anisotropic piezoresistive effect of ReS_2. ACS Nano, 2019, 13: 3310–3319
40 Wagner S, Yim C, McEvoy N, et al. Highly sensitive electromechanical piezoresistive pressure sensors based on large-area layered $PtSe_2$ films. Nano Lett, 2018, 18: 3738–3745